

Copyright

by

Wei Wang

2009

**PLASMONIC PROPERTIES OF SUBWAVELENGTH
STRUCTURES AND PLASMONIC OPTICAL DEVICES**

by

Wei Wang, B.S.

Thesis

Presented to the Faculty of the Graduate School of

The University of Texas at Austin

in Partial Fulfillment

of the Requirements

for the Degree of

Master of Science in Engineering

The University of Texas at Austin

August, 2009

**PLASMONIC PROPERTIES OF SUBWAVELENGTH
STRUCTURES AND PLASMONIC OPTICAL DEVICES**

**Approved by
Supervising Committee:
Shaochen Chen**

Li Shi

Dedication

To my family

Acknowledgements

First of all, I would like to sincerely thank my supervisor, Professor Shaochen Chen, for bringing me into his research group and teaching me with his knowledge and wisdom. Under his patient guidance and help, my graduate studies here in his group had become a wonderful journey and the most rewarding experience in my life. I would also like to thank Professor Li Shi for being my thesis committee member and giving his support to my thesis.

I am also grateful to all my lab mates, past and present, for their help and friendship. I would like to give special gratitude to Dr. Arvind Battula, Dr. Dongbing Shao, Dr. Yi Lu, Dr. David Fozdar, Dr. Li-Hsin Han, Shaomin Wu, Daniel Eils and Wande Zhang, for their assistance in my work. In particular, I would like to Dr. Arvind Battula for helping me learn using simulation software and physics. In addition, I would like to thank all the faculty and staff in the Department of Mechanical Engineering.

Moreover, I would like to thank my family for their consistent love and support. I wouldn't have gone this far if it weren't for my family. I would like to thank my parents Shulin Wang and Yanmin Li for their unending encouragement. At last, I am very thankful to my best friend Si, and Feng, Yibo for their support.

August, 2009

Abstract

PLASMONIC PROPERTIES OF SUBWAVELENGTH STRUCTURES AND PLASMONIC OPTICAL DEVICES

Wei Wang, M.S.E.

The University of Texas at Austin, 2009

Supervisor: Shaochen Chen

This thesis proposes a metallic hole array of a rectangular converging-diverging channel (RCDC) shape with extraordinary transmission. We use a three-dimensional (3D) finite element method to analyze the transmission characteristics of two-dimensional metallic hole arrays (2D-MHA) with RCDC. For a straight channel MHA, when the aperture size is reduced, the transmission peaks have a blue-shift. The same result is observed for a smaller gap throat for the RCDC structure. For the rectangular holes with a high length-width ratio, a similar blue-shift in the transmission peaks as well as a narrower full width at half maximum (FWHM) are observed. The asymmetry from the rectangular shape gives this structure high selectivity for light with different polarizations. Furthermore, the RCDC shape gives extra degrees of geometrical variables to 2D-MHA for tuning the location of the transmission peak and FWHM. The tunable

transmission property of this structure shows promise for applications in tunable filters, photonic circuits, and biosensors.

Table of Contents

Table of Contents	viii
List of Figures	x
Chapter 1: Plasmonics properties of subwavelength structures.....	1
1.1 Introduction.....	1
1.2 Plasmons of subwavelength structures	2
1.2.1 Plasmons among nanoparticles.....	2
1.2.2 Plasmons at metal/dielectric boundaries.....	6
1.3 Simulation tools	15
1.4 Applications of surface plasmons	16
1.4.1 Interacting nanoparticles and applications.....	17
1.4.2 Applications of surface plasmons on smooth surfaces	20
1.4.3 High optical transmission through sub-wavelength periodic structures.....	21
1.4 Objectives	24
1.5 Reference	24
Chapter 2: Tunable and polarization-selective THz range transmission properties of metallic rectangular array with a varying hole channel shape.....	27
2.1 Introduction.....	27
2.2 Computational considerations.....	29
2.3 Results and discussions.....	31
2.3.1 Results for different a/b ratios.....	31
2.3.2 Results for different converging angles	34
2.3.3 Results for different metal film thickness.....	35
2.4 Conclusion	37
2.5 References.....	37
Chapter 3: Conclusion and Future Directions.....	40
3.1 Summary	40
3.2 Future work.....	41

3.3 References.....	42
Bibliography	43
Vita	48

List of Figures

Figure 1.1: Calculated absorption spectrum of a thin gold film (blue dots) and of 30-nm Au nanoparticles in water (red dots) using classical electromagnetic theory. A measured absorption spectrum of an aqueous solution of 30-nm Au colloids (black dots) shows good agreement with the theory. [6]	4
Figure 1.2: S and p-polarized light.....	7
Figure 1.3: P-polarized radiation incidents a surface [9]	8
Figure 1.4: Otto geometry	12
Figure 1.5: Form of the reflectivity curve for p-polarized and s-polarized radiation ($\lambda=632.8\mu\text{m}$) from thick gold and silver films with a sapphire prism ($n = 1.766$). Here the coupling gap is $0.5\mu\text{m}$ for gold and $1.0\mu\text{m}$ for silver. [9].	13
Figure 1.6: Kretschmann-Raether geometry	13
Figure 1.7: Mixed hybrid arrangement.....	14
Figure 1.8: Phase-matching of light to SPPs using a grating [11].	14
Figure 1.9: Measured extinction spectrum (a) and plasmon decay time (b) for regular two dimensional square arrays of Au nanoparticles [6]	18
Figure 1.10: Measured spectral position of the collective plasmon resonances of one dimensional arrays of closely spaced Au nanoparticles for longitudinal (L) and transverse polarizations (T). Also shown are results of a simple near-field point-dipolar coupling model (solid lines) and finite-difference time domain simulations (stars). [6]	20
Figure 1.11: Diffraction and typical transmission spectrum of visible light through a subwavelength hole in an infinitely thin perfect metal film.[21]	22
Figure 1.12: Schematic view of the subwavelength holes arrays studied the paper[12]..	23

Figure 1.13: Zero-order transmission spectrum of an Ag array ($a_0 = 0.9\mu\text{m}$, $d = 150$ nm, $t = 200$ nm)	23
Figure 2.1: Side view of the structure. The thickness of the film is t , and there is a rectangular RCDC hole array with a converging angle θ in it.....	30
Figure 2.2: Top surface of the structure. The rectangular hole array is periodic in both the x and y directions, and the periodicity for the two directions are the same ($22\mu\text{m}$). The inset shows the top view of a single rectangular hole, with a and b defined as the long and short sides. The lengths of the two sides are not identical, resulting in an asymmetric structure along the x and y directions.	30
Figure 2.3: Transmittance spectrum with the same hole area and converging angle $\theta = 30^\circ$, but different a/b ratios (a) $a = 16\mu\text{m}$, $b = 12\mu\text{m}$, (b) $a = 18\mu\text{m}$, $b = 10.7\mu\text{m}$, and (c) $a = 20\mu\text{m}$, $b = 9.6\mu\text{m}$. The solid and dashed lines represent the transmissions for different polarizations. The vertical dashed lines denote the wavelength of each peak.....	33
Figure 2.4: Transmissions for different converging angles. The hole area, film thickness and a/b ratio ($16\mu\text{m}/12\mu\text{m}$) remain the same in all cases.	35
Figure 2.5: Transmissions for different metal film thickness. The hole area, converging angle (30°) and a/b ratio remain the same in all cases. The solid and dashed lines represent the transmissions for different polarizations.....	36

Chapter 1: Plasmonics properties of subwavelength structures

1.1 INTRODUCTION

The electromagnetic properties of metal/dielectric interfaces have attracted a vast amount of research effort ever since the work of Mie [1] and Ritchie [2] for small particles and flat interfaces, respectively. Since then, the ability of such structures to sustain coherent electron oscillations known as surface plasmon polaritons (SPPs), has been intensively investigated. In physics definition, plasmon is a quasiparticle resulting from the quantization of plasma oscillations. They are a hybrid of the electron plasma and the photon. Surface plasmons are those plasmons that are confined to surfaces and that interact strongly with light resulting in a polariton. They occur at the interface of a vacuum or material with a positive dielectric constant with that of a negative dielectric constant (usually a metal or doped dielectric) [3]. Thus, plasmons are collective oscillations of the free electron gas at optical frequencies leading to electromagnetic fields confined to the metallic surface.

The definition of plasmon shows it is a strictly quantum mechanical entity, but actually, we can imagine that plasmons propagate like the ripples that spread across the surface of a pond after you throw a stone in the water [4] and in most cases, we can derive many of their important properties directly using Maxwell's Equations. Actually, Maxwell's Equations are the most powerful tools for nowadays' plasmon research. We will discuss the plasmonic property of nanostructures based on this classical model.

After initial studies of this interaction between electrons and photons, there is a lot of work proposed both in the area of the fundamental physics [5] and for applications such as surface-enhanced spectroscopy and enhancement of nonlinear light generation. More recently, the development of nanofabrication techniques such as EBL (electron-

beam lithography), ion-beam milling, and self-assembly [6], has lead to a resurgence of interest in this field, partly due to potential applications for the fabrication of subwavelength optical devices providing the potential to miniaturize the optical components to or even smaller than the size dimensions of their electronic counterparts, i.e., to the sub-100-nm-size regime. The field of plasmonics received another boost with the discovery of novel "metamaterials" —materials in which electron oscillations can result in astounding optical properties. After all the unifying physical processes enabling light localization and guiding in such structures are the above-mentioned SPP excitation, and the name “plasmonics” has been proposed for the subfield of modern optics studying such processes. [6]

1.2 PLASMONS OF SUBWAVELENGTH STRUCTURES

1.2.1 Plasmons among nanoparticles

Long before Gustav Mie [1] published his famous paper “Beiträge zur Optik trüber Medien, speziell kolloidaler Metallösungen” (contributions to the optics of turbid media, particularly solution of colloidal metals) —in which, Mie derived the optical-absorption spectrum by directly solving Maxwell’s equations for the scattering of electromagnetic waves by spherical objects —the property of strong interaction between microscopic metal particles and visible light has been employed for many purposes. Historically, one prominent use of metal nanoparticles was the staining of glass windows and ceramic pottery, which is the Lycurgus cup, made in Byzantine Empire, 4th century A. D. The cup shows a red color when seen in transmitted light and shows a green color when seen in reflected light. This peculiar behavior is due to small Au nanoparticles embedded in the glass, which show a strong optical absorption of light in the green part

of the visible spectrum. The absorption spectrum of gold nanoparticles and thin film are shown in Figure. 1.1 [6].

From the absorption spectrum of Figure 1.1, we can see that Au particles (indeed many kinds of noble metals, such as Ag, Cu) show striking differences compared to their bulk and thin film responses. The absorption spectrum of 30-nm Au nanoparticles in water (red dots) was obtained by directly solving Maxwell's equations for the scattering of electromagnetic waves by spherical objects as carried out by Mie and retaining only the dipolar term [1], which is suitable for nanoparticles with a diameter $d \ll \lambda$, where λ is the wavelength of light in the surrounding medium. Compare this curve with the measured absorption spectrum of an aqueous solution of 30-nm Au colloids (black dots), we can see this quasistatic approximation is in good agreement with measurement data, which has been confirmed via a plethora of studies of the optical response of metallic nanoparticles with a diameter well below λ in solid, liquid, and gaseous environments.

It can be also seen from Figure 1.1 that there are great differences between the absorption spectrum of the thin film and the nanoparticles. The most notable one is there is a narrow peak around 2.25eV (corresponding to wavelength of 620nm). This unique property is result from that all the free electron oscillator strength for absorption is pulled into a dipolar absorption peak around 2.25eV, which is called the dipolar surface plasmon particle resonance. This modified optical response leads to the bright colors of noble-metal nanoparticles [7]. For higher energies above the dipole resonance, the optical absorption of particles and films is similar, due to the dominance of d-sp electronic interband transitions, which are prominent for Au and Cu in the vicinity of the dipole plasmon resonance, but less so for Ag.

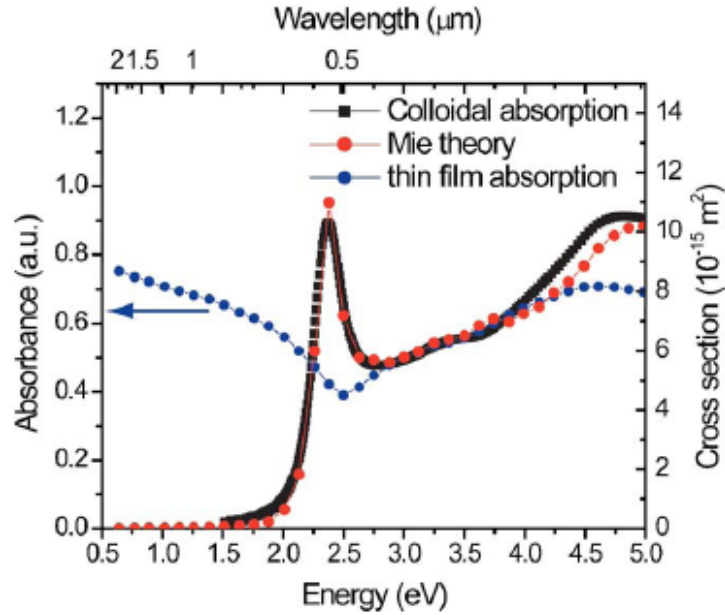


Figure 1.1: Calculated absorption spectrum of a thin gold film (blue dots) and of 30-nm Au nanoparticles in water (red dots) using classical electromagnetic theory. A measured absorption spectrum of an aqueous solution of 30-nm Au colloids (black dots) shows good agreement with the theory. [6]

The unique electromagnetic property of noble-metal nanoparticles is due to the small particle volume. While particles with a diameter $d \ll \lambda$ in the environment with radiation of wavelength λ , the conduction electrons inside the particles all move in phase upon plane-wave excitation which leads to the buildup of polarization charges on the particle surface. The charges then act as a restore force which induces a resonance at certain frequency, say, the particle dipole plasmon frequency. At this specific frequency, the electrons oscillate at a $\pi/2$ phase lag with respect to the driving field, forming a resonant field inside the particle, which in the small particle limit is homogeneous throughout its volume. This resonant field produces a dipolar field outside the particle which leads to enhanced absorption and scattering cross sections for electromagnetic waves, as well as to a strongly enhanced near field in the immediate vicinity of the

particle surface. Indeed, all the special property and applications are based on this dipolar field. [1]

In general, the spectral position, damping, and strength of the dipole and the higher-order plasmon resonances of single metal nanoparticles depend on the particle material, size, geometry, and the dielectric function of the surrounding host [6]. As we know, most of the nanoparticles, whatever man made or naturally, are approximated spheres. Meanwhile there is a theoretical solution for a spheric particle based on Mie's theory. Particularly, for particles with diameter much smaller than the wavelength of encountering light, there is only the lowest (dipolar) order of the modal expansion of the scattered fields has to be retained. In this case this approximate approach achieves excellent agreement with the experiment data, as shown in Figure 1.1. According to Mie's theory, for a spherical metal nanoparticle with radius $a \ll \lambda$, we can get the particle polarizability α [8] :

$$\alpha = 4\pi a^3 \frac{\epsilon - \epsilon_m}{\epsilon + 2\epsilon_m} \quad (1)$$

Where ϵ is the dielectric constant of the nonabsorbing surrounding medium, and $\epsilon = \epsilon(\omega)$ is the dispersive dielectric response of the metal. We can see from this equation, the polarizability achieves its maximum at a certain frequency (Fröhlich frequency), in which case the dominator shows a minimum. The imaginary part of $\epsilon(\omega)$ describes the Ohmic heating losses in the particle, which is due to the collisions of the electrons. Meanwhile, as to larger particles with diameter comparable to larger than the wavelength of incident light, we can not get the same result as small particle. There are two reasons to explain this difference. The first one is retardation effects—the conduction electrons do not all move in phase anymore, leading to a reduced depolarization field at the particle center generated by the surrounding polarized matter. The second one is since we can not

ignore the higher order plasmon resonances any more, the particles could not be considered to be simply dipoles.

1.2.2 Plasmons at metal/dielectric boundaries

When a light encounter a dielectric/metal interface, there may exist at the interface a trapped surface mode which has electro-magnetic fields decaying into both media but which, tied to the oscillating surface charge density, propagates along the interface. This is the surface plasmon. This interaction at interface attract great research because it has a lot of potential applications, including studies of electrochemistry; catalysis; wetting; thin organic condensates as well as solving the resolution limits problem of optical lithography [9]. Before talking about these attractive applications, first however, let's look at some theory to explain the existence of surface plasmon.

1.2.2.1 Simple theory of interaction of electromagnetic radiation with an interface.

To study this interface and the interesting electromagnetic phenomenon we need first to clarify some relatively simple but important concepts of electromagnetism.

The first concept comes to the s and p-polarized light. According to the Maxwell's Equations, for a field without free charges, electromagnetic radiation in isotropic media consists of orthogonal oscillating electric and magnetic fields transverse to the direction of propagation. Then when the radiation passes through a linear polarizer, it will be plane polarized. That means there is a well specified plane in which E or B oscillates, this plane containing the appropriate electromagnetic held vector and the direction of propagation. Now if we consider such radiation falling at an incident angle θ upon a smooth planar interface then we have to consider two important situations.

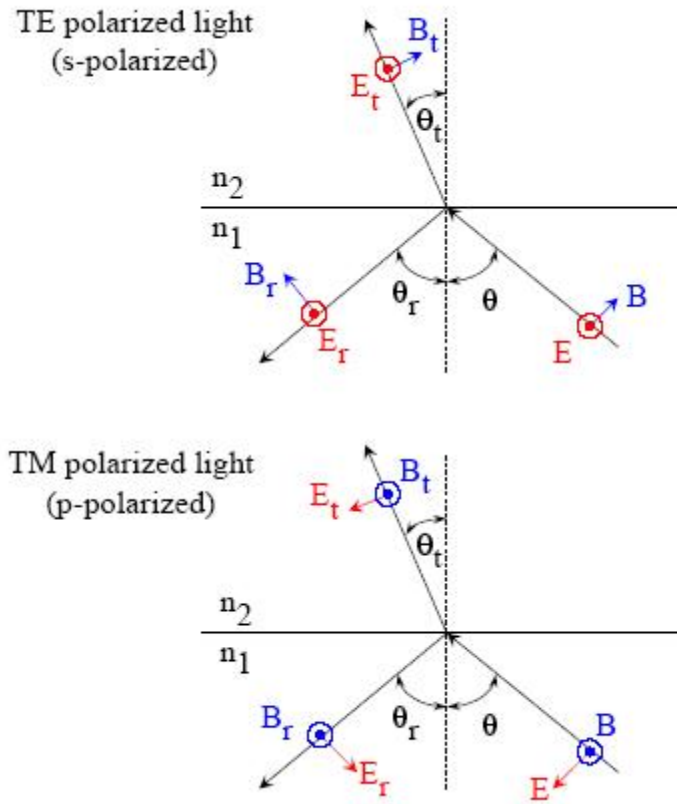


Figure 1.2: S and p-polarized light

As shown in Figure 1.2, in the first case, E vector has only one component, which is tangential to the interface and its B vector has two components one is normal, and the other is tangential, to the interface.

In the second case, B vector has only one component, which is tangential to the interface and its E vector has two components, one is normal and the other is tangential to the interface.

Any linearly polarized radiation may be readily represented by a sum of the above two cases. Since it does not contain normal component, s-polarized incident radiation will not normally cause the creation of charge at a planar interface, while p-polarized radiation will automatically create time dependent polarization charge at the interface.

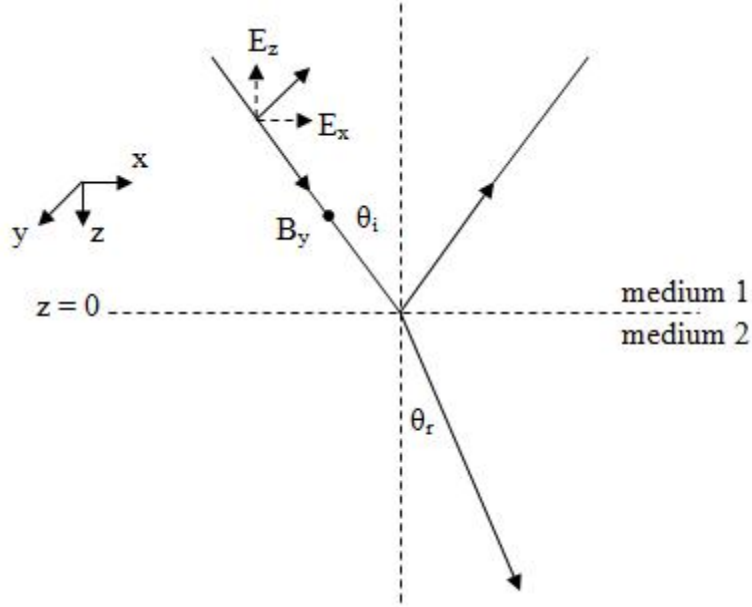


Figure 1.3: P-polarized radiation incidents a surface [9]

The second concept is critical angle. Consider the momentum of photons. For a photon with momentum $\hbar k$, it has momentum $\hbar k_1$ when in a medium of refractive index n_1 . Where $k_1 = k n_1$ is the wavevector in this medium with definition: $k = 2\pi/\lambda$. Assume the z and x components of the momentum of these photons in this medium are $\hbar k_{z1}$ and $\hbar k_{x1}$, respectively. Now these photons travel from this medium to another with refractive index n_2 . For reflected photons, as shown in Figure 1.3, since the refractive index remains the same, say $\hbar|k_1|$ is conserved, and $\hbar k_{x1}$ is conserved for a smooth planar interface, the z component of reflected photons are just simply $-\hbar k_{z1}$. [9]

In the second medium which has a refractive index of n_2 , the radiation propagates in a new direction with momentum $\hbar k_2 = \hbar k n_2$. Since the tangential component of the wavevector conserves when the photons travel through different media, perpendicular component has to change. Now $k_{x1} = k_1 \sin \theta_i$ and $k_{x2} = k_2 \sin \theta_r$, where θ_i and θ_r are the angles of incidence and refraction, respectively. Since $k_{x1} = k_{x2}$, $n_1 \sin \theta_i = n_2 \sin \theta_r$, which is Snell's

law. Supposing the photons travel from a high index medium to a low medium ($n_2 < n_1$), since the maximum of $\sin\theta_r$ is 1, there is a limiting angle of incidence, θ_c , given by

$$\sin \theta_c = n_2/n_1 \quad (2)$$

This angle is called critical angle, beyond which the incident radiation has more momentum along the surface plane than can be supported by medium 2. At this time, all light will be reflected and there is no refractive light. However, for such radiation the oscillating E field will cause the charges in medium 1 and at the interface to oscillate. And this oscillation will induce a radiation penetrating into medium 2. These fields cannot propagate, but are spatially decaying fields (evanescent) which oscillate in time, at the same frequency as the incident radiation, decaying in amplitude in medium 2 in a direction normal to the interface. At the critical angle the decay length is infinite but this falls rapidly to the order of the wavelength of light as the angle of incidence is further increased. This evanescent field for radiation incident beyond the critical angle is useful for coupling radiation to surface plasmons as we shall see later.

Next we consider the boundary conditions of E and B fields. Since there is no boundary orthogonal to E_x , this component is conserved across the boundary. And since there is no free charge at the interface, D_z is continuous. Together with equation $D_z = \epsilon E_z$, we can get the boundary condition of E_z :

$$\epsilon_1 \epsilon_0 E_{z1} = \epsilon_2 \epsilon_0 E_{z2}. \quad (3)$$

1.2.2.2 Detailed theory derived from Maxwell Equations

Based on the discussion above, only p-polarized electromagnetic contributes to the oscillation of the electrons at the interface. As a result we only need to consider this model. If we take the x-y plane to be the interlace plane and the positive z half space as medium 2 as shown in Figure 1.3, the E, B field can be written in the form of wave equation [9]

$$\begin{aligned}
E_1 &= (E_{x1}, 0, E_{z1}) \exp(ik_x x) \exp(ik_{z1} z) \exp(-i\omega t) \\
H_1 &= (0, H_{y1}, 0) \exp(ik_x x) \exp(ik_{z1} z) \exp(-i\omega t) \\
E_2 &= (E_{x2}, 0, E_{z2}) \exp(ik_x x) \exp(ik_{z2} z) \exp(-i\omega t) \\
H_2 &= (0, H_{y2}, 0) \exp(ik_x x) \exp(ik_{z2} z) \exp(-i\omega t)
\end{aligned} \tag{4}$$

Applying Maxwell's Equations $\nabla \cdot E = 0$ and $\nabla \times E = -\mu \frac{\partial H}{\partial t}$, where

$$\begin{aligned}
E_{z1} &= -E_{x1} = \frac{k_x}{k_{z1}} \\
E_{z2} &= -E_{x2} = \frac{k_x}{k_{z2}}
\end{aligned} \tag{5}$$

$$\begin{aligned}
H_{y1} &= \omega E_{x1} \epsilon_1 \epsilon_0 / k_{z1} \\
H_{y2} &= \omega E_{x2} \epsilon_2 \epsilon_0 / k_{z2}
\end{aligned} \tag{6}$$

Then we apply the boundary conditions at $z=0$. According to the discussion above, the tangential H is continuous and so is the tangential E , which leads to the simple equation between the permittivities and the normal component of wavevector below

$$\frac{\epsilon_1}{k_{z1}} = \frac{\epsilon_2}{k_{z2}} \tag{7}$$

Also since $\epsilon_i k^2 = k_x^2 + k_{zi}^2$, $i=1,2$. If the wave is truly a trapped surface wave with exponential decays into both media then we need $ik_{z1} < 0$ and $ik_{z2} > 0$. Thus both k components are imaginary with opposite signs

$$\begin{aligned}
k_{z1} &= -i(k_x^2 - \epsilon_1 k^2)^{1/2}, \text{ requiring } k_x^2 > \epsilon_1 k^2 \\
k_{z2} &= i(k_x^2 - \epsilon_2 k^2)^{1/2}, \text{ requiring } k_x^2 > \epsilon_2 k^2
\end{aligned} \tag{8}$$

So relative permittivities in two media are of opposite sign. The first condition tells us the surface mode wavevector is greater than the maximum photon wavevector available in the dielectric. The second condition, for the metal, is automatically satisfied with relative permittivity negative.

Substituting expressions (8) into (7) to give:

$$k_x = k \left(\frac{\epsilon_1 \epsilon_2}{\epsilon_1 + \epsilon_2} \right)^{1/2} \quad (9)$$

Where ϵ_2 (relative permittivity in metal) is a complex number with a real component $\epsilon_{2r} < 0$ and an imaginary part ϵ_{2i} .

So the wavevector is also a complex number:

$$k_x = k \left[\frac{\epsilon_1 (\epsilon_{2r} + i \epsilon_{2i})}{\epsilon_1 + \epsilon_{2r} + i \epsilon_{2i}} \right]^{1/2} \quad (10)$$

with a real component $k_{xr} \cong k \epsilon_1^{1/2} \left(1 - \frac{\epsilon_1}{2 \epsilon_{2r}} \right)$ and an imaginary component $k_{xi} = \frac{1}{2} k \frac{\epsilon_{2i} \epsilon_1^{3/2}}{\epsilon_{2r}^2}$ [9]. The imaginary component of the wavevector is related with the propagation length of the surface plasmon.

Form equation (9), we can see that for k_x to be real, the requirement is $|\epsilon_{2r}| > \epsilon_1$. This equation also tells us that the interaction between the surface charge density and the electromagnetic field results in the momentum of the SP mode, k_x , being greater than that of a free-space photon of the same frequency, k which is the free-space wavevector. So it is a big issue to provide this extra momentum to take advantage of surface plasmon. The techniques providing the missing momentum will be discussed below.

1.2.2.3 Techniques to excite the surface plasmons

In this section, we will concentrate on two techniques used to take advantage of surface plasmon at the dielectric/metal interface. The main idea of the first one is to make use of prism coupling to enhance the momentum of the incident light at the smooth interface [10]. The second one involves utilizing the gratings to excite the surface plasmons [11].

The use of prism is to produce enhanced momentum of photons in the dielectric medium. To better explain the method, we have to refer to the concept of critical angle

introduced before. We know that beyond the critical angle of incidence there will be an evanescent field in the second half space. This evanescent field does not propagate, but has a momentum in the x direction, which is $n_1 \hbar k \sin \theta_i$, since $\theta_i > \theta_c$, $n_1 \hbar k \sin \theta_i > n_2 \hbar k$. Where the enhancement of momentum in the dielectric medium is $n_1 \hbar k \sin \theta_i - n_2 \hbar k = n_1 \hbar k (\sin \theta_i - \sin \theta_c)$, which could be used to couple radiation to surface plasmon. As a result it is possible to place the metal/dielectric interface which supports the surface plasmon close enough to the totally internally reflecting interface. An obvious geometry to consider is that shown in figure 1.4, which is called Otto geometry. [9-10]

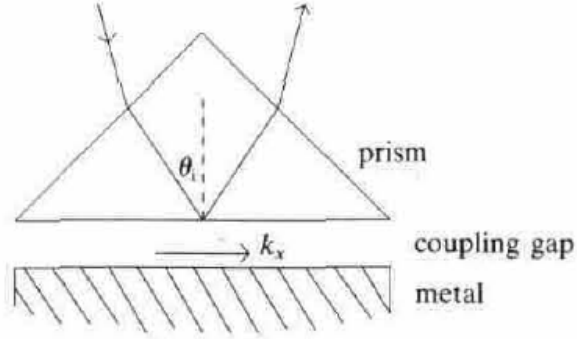


Figure 1.4: Otto geometry

We can see from figure 1.4 that by varying the incident angle from the prism, we can get an x-component of electric field larger than it can be sustained in the air gap (or a space with low index). Then there will be an evanescent electric field in the gap as we mentioned before. This field will excite the surface plasmon at the air (dielectric) metal interface. The air gap is less than a few radiation wavelengths thick (for visible $< 2\mu\text{m}$). The form of the reflectivity curve for gold and silver at 632.8 nm is shown in figure 1.5 [9]. We can also see the curve for s-polarized radiation which is not capable of creating the surface plasmon.

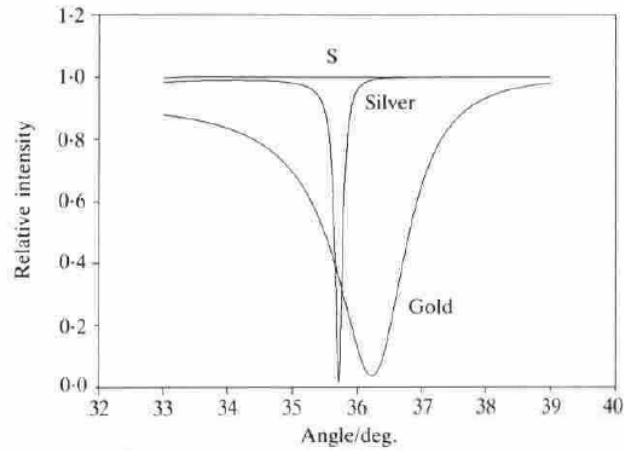


Figure 1.5: Form of the reflectivity curve for p-polarized and s-polarized radiation ($\lambda=632.8\mu\text{m}$) from thick gold and silver films with a sapphire prism ($n = 1.766$). Here the coupling gap is $0.5\mu\text{m}$ for gold and $1.0\mu\text{m}$ for silver. [9]

A very obvious disadvantage of Otto geometry is that it is difficult to fabricate the air gap. This problem may be addressed in quite a different manner by using, instead of an air gap, an evaporated dielectric spacing layer (or perhaps a spun polymer). Figure 1.6 and 1.7 illustrate examples of substitutions of Otto geometry. [9]

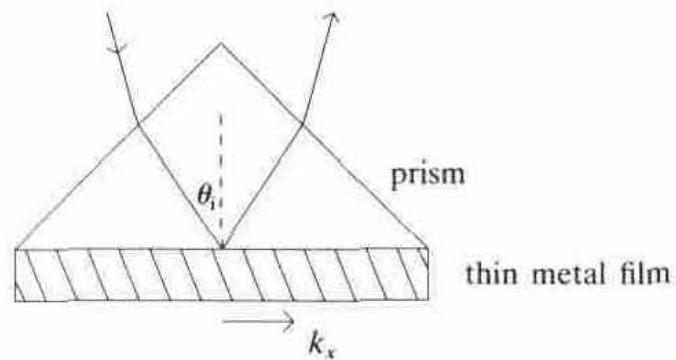


Figure 1.6: Kretschmann-Raether geometry

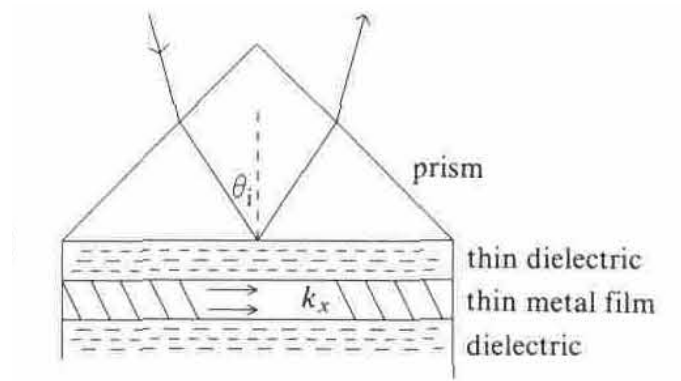


Figure 1.7: Mixed hybrid arrangement

The mismatch in wave vector between the in-plane momentum $k_x = k \sin \theta$ of impinging photons can also be achieved by patterning the metal surface with a shallow grating of grooves or holes with lattice constant (periodicity) a . As shown in figure 1.8, for the simple one-dimensional grating of grooves, phase matching takes place:

$$k_{sp} = k_x \pm 2n\pi / a \quad (11)$$

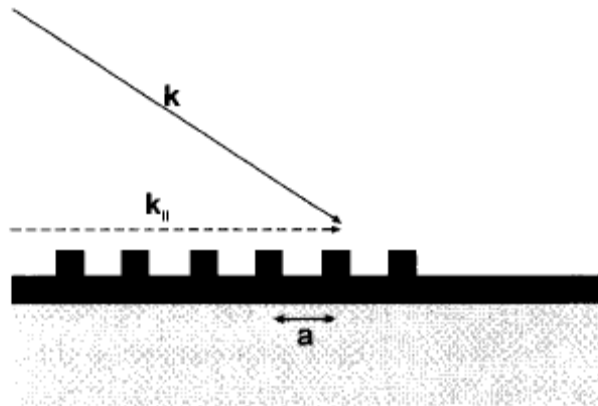


Figure 1.8: Phase-matching of light to SPPs using a grating [11].

Where k_{sp} is the wavevector of the surface plasmon $k_{sp} = k_0 \frac{1}{\sqrt{1 + (1/\epsilon_m)}}$, k_x is the in-plane wavevector $k_x = k \sin \theta$, a is the lattice constant (periodicity), and $n = (1, 2, 3, \dots)$. As with prism coupling, excitation of SPPs is detected when the reflected light is at minimum. Surface plasmon excited by grating dielectric/metal interface attracted intensive interest these years since Ebbesen et al. first reported that a thin metal film perforated with an array of subwavelength sized holes can transmit much more light than expected [12], which will be described in the next section.

1.3 SIMULATION TOOLS

Since sometimes the mechanism of surface plasmon could not be explained by existing theory, we have to use numerical simulation to predict the distribution of an electric field in a nanostructure. Two methods—FDTD (finite difference time domain) and Finite-Element Method are frequently used in simulation, which we will discuss below.

The FDTD method solves the Maxwell's equations and it became feasible after Yee's elegant discretization algorithm [8]. Since then it has been widely used as a fundamental tool in microwave engineering and recently FDTD finds its way into near-field optics. The mechanism of this method is to divide the whole space into a series of small grids, and then the Maxwell Equations could be transformed into difference form for each grid. Solving this set of finite difference equations, one can get numerical solution of the electric field in the whole space.

The finite element method (FEM) is used for finding an approximate solution of partial differential equations (PDE) as well as of integral equations such as the heat transport equation. The solution approach is based either on eliminating the differential equation completely (steady state problems), or rendering the PDE into an equivalent

ordinary differential equation, which is then solved using standard techniques such as finite differences, etc [13]. There are already some commercial software available for solving the electric field using FEM, such as FEMLAB®(COMSOL®), ANSYS®, etc. In FEMLAB®(COMSOL®), for solving the electric field, one only needs to set the coefficients of the PDE and boundary conditions.

1.4 APPLICATIONS OF SURFACE PLASMONS

Surface plasmons, as we mentioned above, is a phenomenon we can use to manipulate the flow of light in nanoscale. With different elaborately designed structure, one can use surface plasmons to manipulate light for different purposes. Research in this area could lead to an entirely new class of optical devices. Ultimately it may be possible to employ plasmonic components in a wide variety of instruments, with their help we will be able to improve the resolution of microscopes, the efficiency of light-emitting diodes (LEDs) and the sensitivity of chemical and biological detectors. Scientists are also considering medical applications, designing tiny particles that could use plasmon resonance absorption to kill cancerous tissues, for example. Some researchers have even theorized that certain plasmonic materials could alter the direction of light around an object to such an extent that it would become invisible—the technology that may make invisibility cloaks a reality.

Plasmonics, along with the developments of computational power—which have enabled investigators to accurately simulate the complex electromagnetic fields generated by plasmonic effects, and novel methods for constructing nanoscale structures—which have made it possible to build and test ultrasmall plasmonic devices and circuits improve our understanding of light and extend our ability to utilize light in a boarder range. In the following part of this thesis, I will introduce some important and interesting applications. Again, here we have to select a rather small amount of topics for this review.

1.4.1 Interacting nanoparticles and applications

The progress of particle synthesis and fabrication techniques provides more opportunities to take advantage of the unique properties of nanoparticles. Nowadays, we can arrange the nanoparticles in ordered array. Since each particle with a diameter much smaller than the wavelength of incident light could be considered to be a dipole, the interaction among nanoparticles becomes the interaction among dipoles. Thus, by now, two kinds of arrangements—depending on the spacing between two adjacent particles--have been intensively investigated. The first arrangement is that the spacing is on the order of the wavelength. In this case, the far-field dipolar interaction dominates. Figure 1.9 [8, 14] shows an example of the dependence of both extinction peak and plasmon decay time on the grating constant d for a regular square array of 150-nm-diameter Au nanoparticles. Both the variation of the spectral position and width of the resonances can be explained by assuming far-field dipolar interactions. The arrangement could be used for maximizing surface-enhanced Raman scattering of adsorbed molecules. [14]

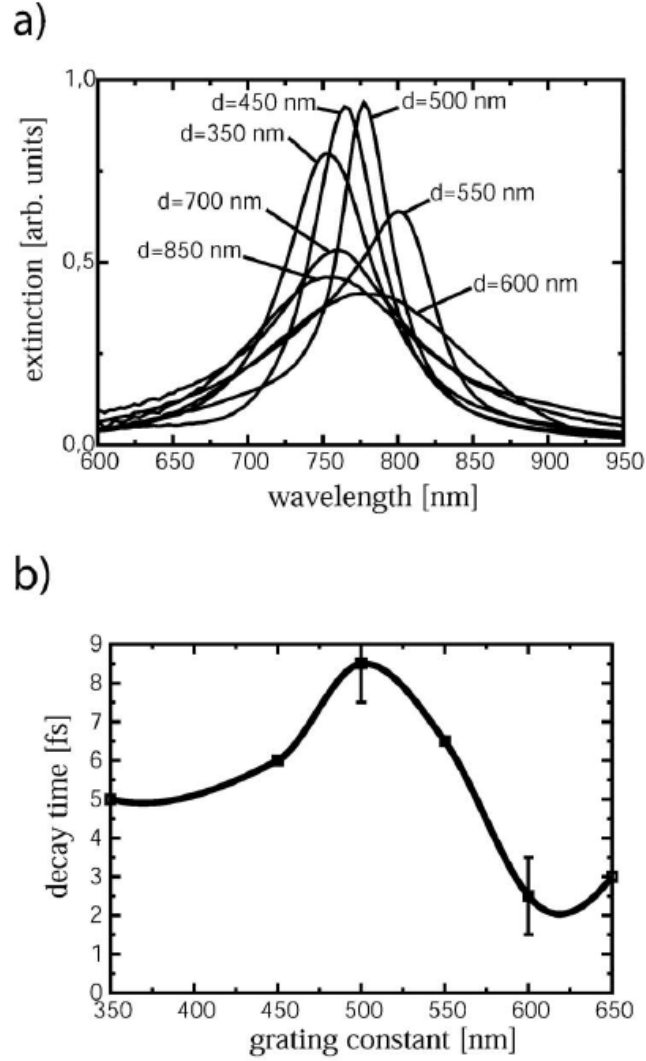


Figure 1.9: Measured extinction spectrum (a) and plasmon decay time (b) for regular two dimensional square arrays of Au nanoparticles [6]

The enhanced near fields around metallic nanostructures induced by illumination at visible and near-infrared frequencies allow for a variety of intriguing applications apart from energy guiding in ordered particle arrays discussed above. Since the enhanced fields are localized on the surface of the nanostructures, they serve as a local probe of the dielectric environment within a few nanometers of the particle surface. This fact has, for

example, been employed in studying variations of the local refractive index in light of biological (mass) sensing applications. Also, the local response of metallic nanostructures can serve so as to enhance the incoming and generated fields for nonlinear processes and decay rate enhancements of emissive species. [14]

The second arrangement is that the particle spacing is much smaller than the wavelength of light. In this case, the near-field dipolar interaction dominates. These strongly distance-dependent interactions lead to a splitting of the plasmon. Figure 1.10 [14] shows dipolar peak for regular one-dimensional arrays of 50-nm Au particles. The spectral position of the extinction peak for far-field excitation shows a blueshift for polarization perpendicular to the chain axis (T), and a redshift for longitudinal polarization (L), which can easily be understood by analyzing Columbic force interactions between the electrons in neighboring particles. One application of near-field coupling between particles in ordered arrays is the use of such structures as waveguides for electromagnetic energies at optical frequencies with a lateral mode profile below the diffraction limit of light. [14]

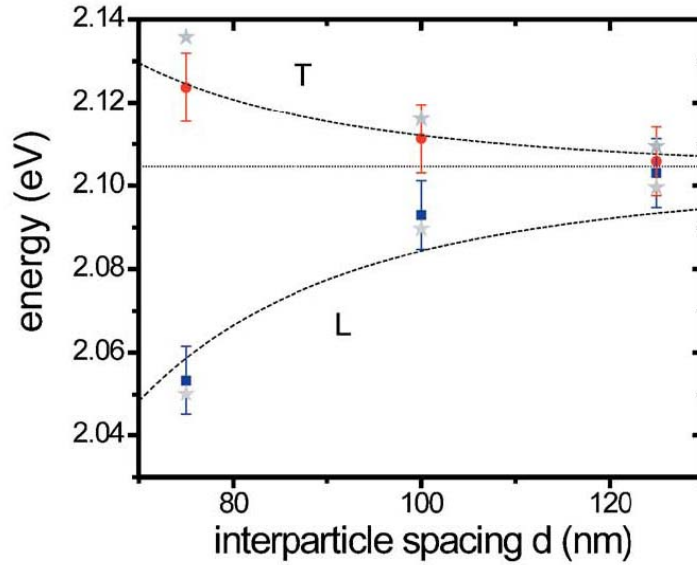


Figure 1.10: Measured spectral position of the collective plasmon resonances of one dimensional arrays of closely spaced Au nanoparticles for longitudinal (L) and transverse polarizations (T). Also shown are results of a simple near-field point-dipolar coupling model (solid lines) and finite-difference time domain simulations (stars). [6]

1.4.2 Applications of surface plasmons on smooth surfaces

From the analysis in the last section, we can see that the momentum of the surface plasmon, which is readily monitored by coupling incident radiation to it, is easily changed by thin layers of material deposited on the metal surface [15] or by small changes in the dielectric constant of the material adjacent to the metal. One of the simplest applications for this phenomenon is to examine the chemical contamination of the metal by checking the surface plasmon it supports. For example it is simple by monitoring the surface plasmon resonance of silver in the Kretschmann-Raether geometry to observe the progressive growth of silver sulphide on exposure to the atmosphere. By monitoring the shift in resonance angle over many days, Kovacs[16] found for this particular environment that 2 nm of silver sulphide formed after about

thirty days of exposure. It has more interesting and important application in deliberately overcoating the surface plasmon supporting metal, the active medium, with other types of layers. For example, when depositing organic multilayers using the Langmuir-Blodgett technique, well-defined stepped structures may be fabricated by careful control of the deposition of these layers. For these the angular dependent reflectivity for the Kretschmann-Raether geometry shows a surface plasmon resonance which steps progressively to a higher angle as the layer thickness is stepped integrally [17]. This then allows determination of the assumed isotropic relative permittivities and thicknesses of the organic overlayers.

Other than sensors, there is a perceived potential for device application in other areas. For example, fiber polarizers with very high extinction ratios have already been fabricated in which thin metal layers provide the necessary surface plasmon resonance absorption thus destroying one polarization component [18]. There is also interest in the use of surface plasmon excitation in scanning surface microscopy [9]. Small variations in overlayers on an active metal film are easily converted into large differences in reflectivity by setting the system at the angle of the surface plasmon excitation and scanning across the sample.

Another important potential application for the use of surface plasmons is non-linear optics. The optical excitation of this surface-travelling wave resonance results in strong enhancement of the electromagnetic field at the surface supporting the surface plasmon. This gives substantial potential for the study of strong optical field effects[9] as well as strong non-linear effects due to local heating[19-20].

1.4.3 High optical transmission through sub-wavelength periodic structures

When light scatters through apertures, it diffracts at the edges. In the subwavelength regime, Bethe was able to give a theoretical description of the diffraction

of light at a given wavelength λ through a circular hole of radius $r \ll \lambda$ in the idealized situation of an infinitely thin and perfect metal sheet. He has shown that the transmission $T(\lambda)$ scales uniformly with the ratio of r to λ to the power of four, as described in equation (12) and schematically shown below in figure 1.11.[21]

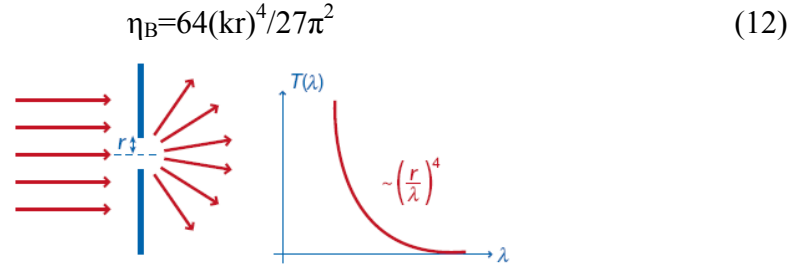


Figure 1.11: Diffraction and typical transmission spectrum of visible light through a subwavelength hole in an infinitely thin perfect metal film.[21]

We can see that when the scale of the hole is smaller than the wavelength of the incident light, the amount of transmission light will be very small. However, recently, several experiments have shown that, if holes are structured forming a 2D periodic array in a metallic film, extraordinary optical transmission can be obtained at wavelengths up to 10 times larger than the diameter of the holes [12]. Figure 1.12 shows the geometry literature [12] used to achieve the high transmission.

Typically, a silver film of thickness $t=0.2\mu\text{m}$ was first deposited by evaporation on a quartz substrate. Arrays of cylindrical holes were fabricated through the film by using a focused-ion-beam (FIB). The individual hole diameter d was varied between 150nm and 1 mm and the spacing between the holes (that is, the periodicity) a_0 , was between 0.6 and 1.8mm [12].

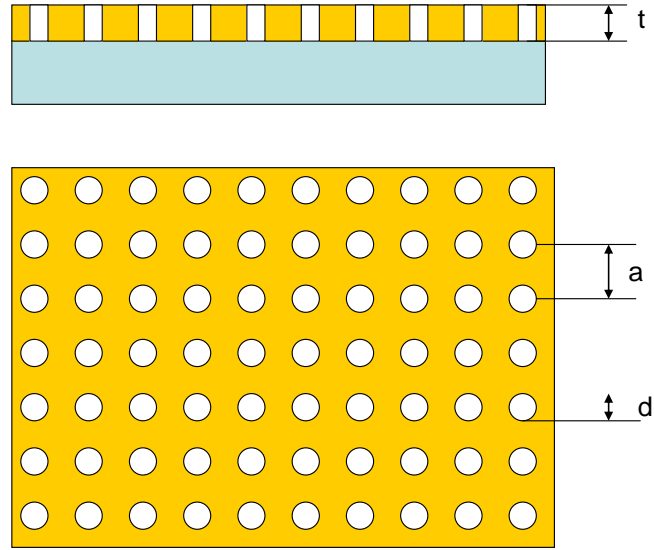


Figure 1.12: Schematic view of the subwavelength holes arrays studied the paper[12]

Figure 1.13 shows a zero-order transmission spectrum for a square array of 150nm holes with a period a_0 of $0.9\mu\text{m}$ in a 200nm thick Ag film [12].

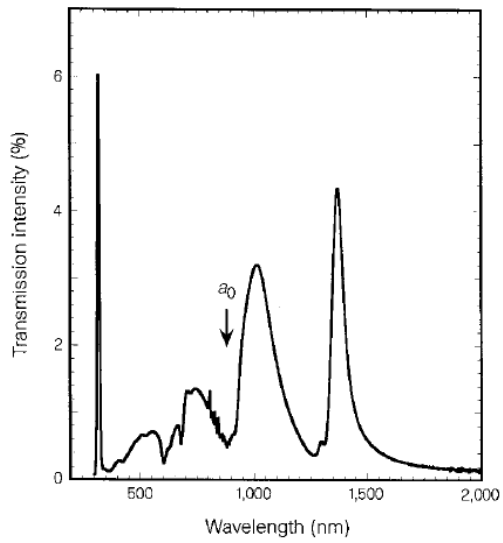


Figure 1.13: Zero-order transmission spectrum of an Ag array ($a_0 = 0.9\mu\text{m}$, $d = 150\text{ nm}$, $t = 200\text{ nm}$)

Fig.1.13 shows a number of distinct features. The first one is at wavelength $\lambda=326\text{nm}$, the narrow bulk silver plasmon peak is observed. But as the film becomes thicker, this peak will disappear. The second as well as the most remarkable one is the set of peaks which become gradually stronger at longer wavelengths, increasingly so even beyond the minimum at the periodicity a_0 .

1.4 OBJECTIVES

The goals of this thesis are to design and analyze plasmonic optical devices. To understand the plasmonic nature of the optical devices both designed numerical computation using Finite Element Method (FEM) and theoretical computation based on Mie theory were performed.

Chapter 2 is about polarization selective extraordinary transmission (EOT) through subwavelength holes and apertures in metallic films. It will be discussed on how the EOT spectral locations can be tuned by introducing an extra degree of freedom in the geometrical parameter.

1.5 REFERENCE

1. Mie, G., Articles on the optical characteristics of turbid tubes, especially colloidal metal solutions. *ANNALEN DER PHYSIK* 1908(25).
2. Ritchie, R.H., Plasma losses by fast electrons in thin films. *PHYSICAL REVIEW* 1957(106).
3. Wikipedia. Plasmon. Available from: <http://en.wikipedia.org/wiki/Plasmonics>.
4. Atwater, H.A., The promise of plasmonics. *Scientific American*, 2007. 296(4): p. 56-63.
5. Raether, H., *Surface Plasmons on Smooth and Rough Surfaces and on Gratings*. 1988: Springer-Verlag. 136 pages.
6. Maier, S.A. and H.A. Atwater, Plasmonics: Localization and guiding of electromagnetic energy in metal/dielectric structures. *Journal of Applied Physics*, 2005. 98(1).

7. Mulvaney, P., Not all that's gold does glitter. *Mrs Bulletin*, 2001. 26(12): p. 1009-1014.
8. Yee, K.S., Numerical solution of initial boundary value problems involving Maxwell' s equations in isotropic media. *IEEE Trans. Antennas Propag.*, 1966(14).
9. Sambles, J.R., G.W. Bradbery, and F.Z. Yang, Optical-Excitation of Surface-Plasmons - an Introduction. *Contemporary Physics*, 1991. 32(3): p. 173-183.
10. OTTO, A., EXCITATION OF NONRADIATIVE SURFACE PLASMA WAVES IN SILVER BY METHOD OF FRUSTRATED TOTAL REFLECTION. *ZEITSCHRIFT FUR PHYSIK*, 1968(216): p. 398.
11. Maier, S.A., *Plasmonics: Fundamentals and Applications*. 1 edition ed. 2007: Springer. 223.
12. Ebbesen, T.W., et al., Extraordinary optical transmission through sub-wavelength hole arrays. *Nature*, 1998. 391(6668): p. 667-669.
13. Wikipedia. Finite element method. Available from: http://en.wikipedia.org/wiki/Finite_Element_Method.
14. Yee, S.S., J. Homola, and G. Gauglitz, Special issue: Surface plasmon resonance (SPR) optical sensors, current technology and applications - Preface. *Sensors and Actuators B-Chemical*, 1999. 54(1-2): p. 1-1.
15. Pockrand, I., Surface Plasma-Oscillations at Silver Surfaces with Thin Transparent and Absorbing Coatings. *Surface Science*, 1978. 72(3): p. 577-588.
16. Kovacs, G.J., Sulfide Formation on Evaporated Ag Films. *Surface Science*, 1978. 78(1): p. L245-L249.
17. Brown, C.A., et al., Unusual Monolayer Behavior of a Geminally Disubstituted Fatty-Acid - Characterization Via Surface-Plasmons and X-Ray Photoelectron-Spectroscopy Study. *Journal of Physical Chemistry*, 1983. 87(19): p. 3616-3619.
18. Johnstone, W., et al., Fibre-Optic Polarizers and Polarizing Couplers. *Electronics Letters*, 1988. 24(14): p. 866-868.
19. Martinot, P., S. Laval, and A. Koster, Optical Bistability from Surface-Plasmon Excitation through a Nonlinear Medium. *Journal De Physique*, 1984. 45(3): p. 597-600.

20. Innes, R.A. and J.R. Sambles, Optical Non-Linearity in Liquid-Crystals Using Surface Plasmon-Polaritons. *Journal of Physics-Condensed Matter*, 1989. 1(35): p. 6231-6260.
21. Genet, C. and T.W. Ebbesen, Light in tiny holes. *Nature*, 2007. 445(7123): p. 39-46.

Chapter 2: Tunable and polarization-selective THz range transmission properties of metallic rectangular array with a varying hole channel shape

2.1 INTRODUCTION

In 1998, extraordinary optical transmission (EOT) phenomenon was reported by T. W. Ebbesen and his coworkers. EOT was achieved through subwavelength metallic hole arrays (MHAs) milled in an opaque metal screen [1]. This work generated considerable interest and led to the development of a new family of optical devices based on subwavelength hole arrays with tunable transmission spectrums via adjustable array properties (periodicity, thickness of the film, etc.). There have been arguments about the main cause of this high transmission through subwavelength holes [2-4]; however, more and more researchers in this area are beginning to believe that enhanced transmission through subwavelength MHA can be divided into three steps: the coupling of light to SPPs on the incident surface, the transmission through the holes and the re-emission from the second surface. EOT in the terahertz (THz) region has been observed recently in both metallic [5-8] and semiconductor hole arrays [9-11]. Although metal surfaces in this frequency region act as perfect conductors and the SPPs excitation cannot be expected, it has been proven both experimentally [12] and theoretically [13] that the resonantly-excited SPP-like mode plays an important role in high transmission in the THz region.

Photonic structures have several geometric variables, such as film thickness, interface media, periodicity, hole shape, aperture size, etc., that can be used to manipulate the light propagation at the subwavelength scale. As mentioned above, the high transmission is caused by the coupling interaction of the SPPs on both the incident and the transmitted surfaces and is strongly affected by the thickness of the metal film. The

transmission decreases exponentially with increasing depth [14], and the SPPs on the two surfaces are uncoupled when the hole depth is large. It is observed in the THz region that the EOT can be achieved at an array thickness of only one third of the skin depth [15]. It has also been shown that the peak transmission has a red-shift as the index of refraction inside the metallic hole arrays undergoes an increase [16]. Similarly, when the surrounding dielectric constant increases, a red-shift along with a reduction in the transmission magnitude is observed [9]. In addition to the parameters that have already been discussed, periodicity is also very important. It has been reported that a planar circular grating with the period of the rings matching the SPP wavelength can have enhanced intensity at the focal point of the plasmonic lens [17]. Different hole shapes have also been studied. A circular hole shape has an order of magnitude higher normalized transmission than a rectangular shape, along with a large blue-shift spectrum [18]. Also, the different influence of the hole shape in the THz region from that in the optical region has been studied [5, 6].

The hole size along with the channel shape will have significant impact on the transmission efficiency because the holes are expected to mediate the SPP coupling between both surfaces of the metal film. Recently we have proposed a subwavelength hole array having a converging diverging channel (CDC) with a circular hole shape [19]. This CDC-shaped hole array offers similar EOT effects, yet has an extra degree of freedom in a geometric variable, the converging angle, to tune the transmission spectrum. The converging angle determines the slope of the sidewall and the area at the throat of the CDC channels (Fig. 2.1). The transmission spectrum was studied for a 2D-MHA with variable throat and aperture size and was compared with a straight channel array. The results show that when the channel shape is changed to CDC the transmittance peaks

become narrower and there is a blue-shift. The blue-shift becomes larger as the throat area decreases.

In this work, we propose to use a rectangular converging-diverging channel (RCDC) to study the EOT properties for light with different polarizations. The proposed structure has another geometric variable, the length-width ratio of the rectangle that can be used to tune the transmission properties. More importantly, this structure has a strong selectivity for different polarizations.

2.2 COMPUTATIONAL CONSIDERATIONS

Figure 2.1 shows a side view of the structure used for the simulation where the incident light goes through a thin film of silver. The thickness of the film is t , and there is a rectangular RCDC hole array with a converging angle θ in it. The transmission vs. wavelength curve was calculated for different geometric variables. Figure 2.2 shows the top surface of the silver film. The rectangular hole array is periodic in both the x and y directions, and the periodicity for the two directions are the same ($22\mu\text{m}$). The inset shows the top view of a single rectangular hole, with a and b defined as the long and short sides. The lengths of the two sides are not identical, resulting in an asymmetric structure along the x and y directions. Transmissions are expected to change with different polarizations of the incident light. In fact, we will show that such a structure has a very high selectivity of transmission with different polarizations and can be used as a polarization-selective filter.

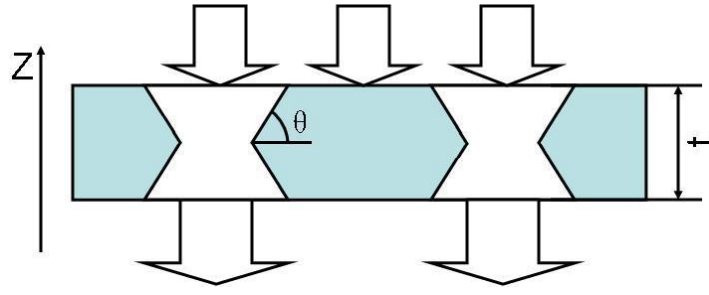


Figure 2.1: Side view of the structure. The thickness of the film is t , and there is a rectangular RCDC hole array with a converging angle θ in it.

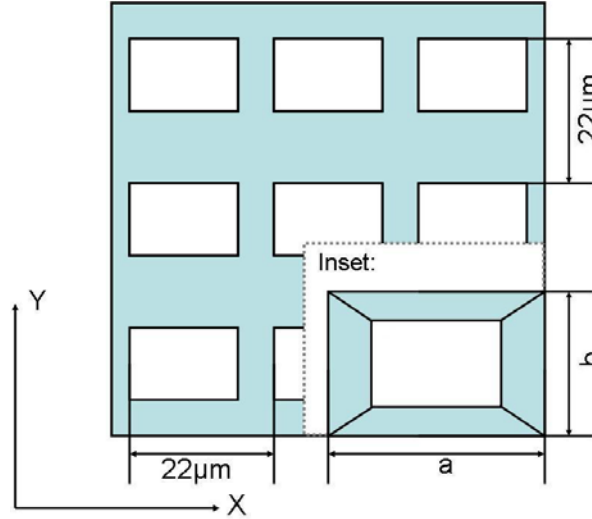


Figure 2.2: Top surface of the structure. The rectangular hole array is periodic in both the x and y directions, and the periodicity for the two directions are the same ($22\mu\text{m}$). The inset shows the top view of a single rectangular hole, with a and b defined as the long and short sides. The lengths of the two sides are not identical, resulting in an asymmetric structure along the x and y directions.

In this chapter, we will change the length-width ratio (a/b), the converging angle θ , and the metal film thickness t , while keeping the other parameters unchanged to study the effect of these parameters on the relationship between transmission and wavelength.

For this study we considered the frequency to be around 15 THz or $20\mu\text{m}$ wavelength. The dielectric constant of silver used in the simulation was described by the Drude model $\varepsilon = \varepsilon_{\infty} - \omega_p^2 / (\omega^2 + i\gamma\omega)$, where $\varepsilon_{\infty} = -175.0$, $\omega_p = 1.1 \times 10^{16} \text{ s}^{-1}$, and $\gamma = 10.51 \times 10^{13} \text{ s}^{-1}$ [20]. The electromagnetic fields were assumed to be time harmonic and the resulting governing equations for the steady-state distribution was solved using a commercially available 3-dimensional (3D) finite element software (COMSOL 3.3) [21]. The computational domain considered is a single unit cell surrounded either by periodic boundary conditions or by perfectly matching layers (PML) [22].

2.3 RESULTS AND DISCUSSIONS

2.3.1 Results for different a/b ratios

Figure 2.3 (a-c) shows the transmission spectrums for Ag MHAs having different a/b ratios. For all the cases, the hole area, the converging angle (30°) and the metal film thickness ($2\mu\text{m}$) are kept the same. The solid and dashed lines show the transmissions for different polarizations (solid line: E-field parallel to the short side; dash line: E-field parallel to the long side). Since these 2D structures are asymmetric along their short and long sides, the polarization becomes a very crucial parameter for the transmission peak. In the case of polarization (i.e., E-field) parallel to the long sides of the rectangles, there is negligible transmission. When the incident polarization is rotated 90° to point along the rectangles' minor sides, the aperture transmits a substantial fraction of the incident light, in agreement with the result reported previously [23].

The transmission spectrum changes as the a/b ratio increases, but the magnitude of the transmission peak remains the same and is much larger than $(A/\lambda)^4$, the Bethe-Bouwkamp power law model. In this model, 'A' is the aperture size and ' λ ' is the wavelength of the light. By changing the a/b ratio, we can tune the position of the band and the full width at half maximum (FWHM). For example, decreasing the a/b ratio causes an increase in the FWHM of the transmission peaks accompanied by a red-shift. At the frequencies below the cutoff frequency ω_c (the frequencies at which the transmission reaches half maximum of the peak), the curves are very sharp and the transmissions rapidly drop to 0.1. This means the RCDC structures with different a/b ratios are all very good filters for low frequencies.

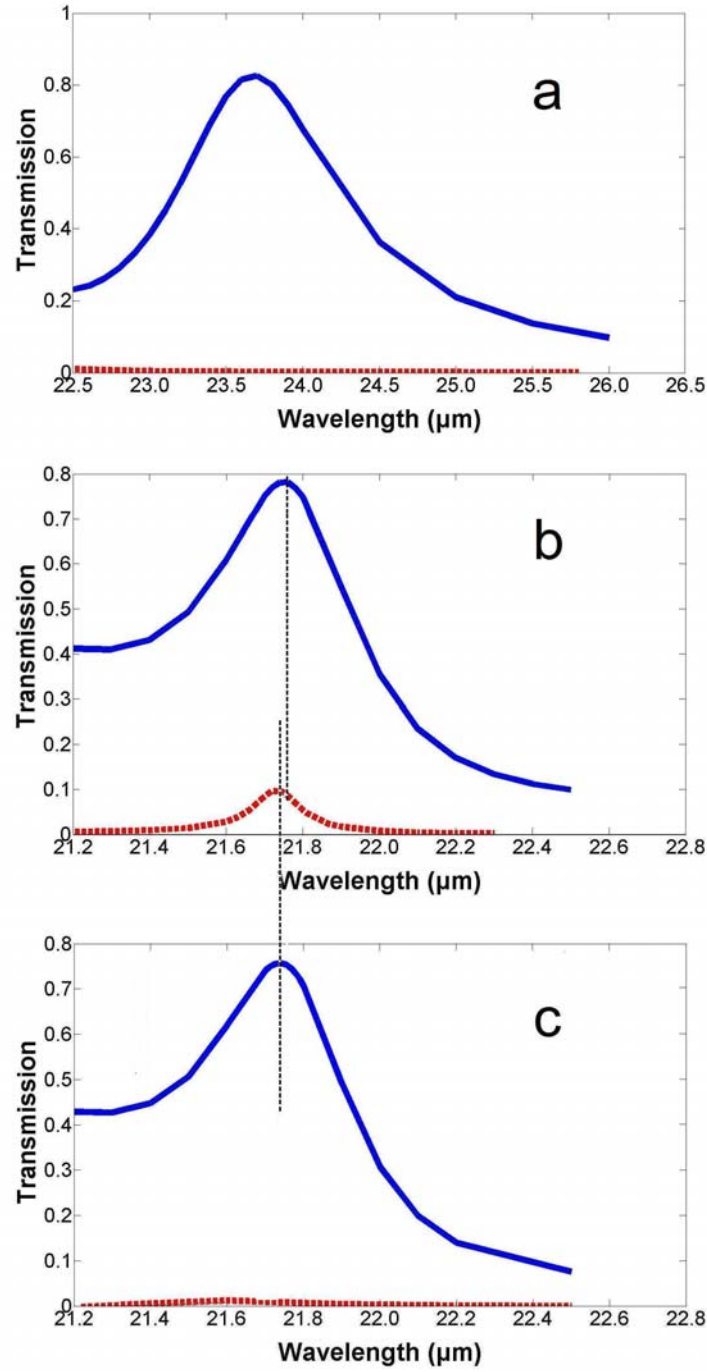


Figure 2.3: Transmittance spectrum with the same hole area and converging angle $\theta=30^\circ$, but different a/b ratios (a) $a=16\mu\text{m}$, $b=12\mu\text{m}$, (b) $a=18\mu\text{m}$, $b=10.7\mu\text{m}$, and (c) $a=20\mu\text{m}$, $b=9.6\mu\text{m}$. The solid and dashed lines represent the transmissions for different polarizations. The vertical dashed lines denote the wavelength of each peak.

2.3.2 Results for different converging angles

Figure 2.4 shows the transmission spectrum for Ag MHAs with different converging angles while keeping the same hole area, a/b ratio (16 μ m/12 μ m) and film thickness (2 μ m). The two sets of simulation data show a high-selectivity for different polarizations. Similar to the results in section 3.1, the transmission spectra for an E-field perpendicular to the long side has a strong peak for each converging angle in this wavelength range, while there is no peak in the range of our interest for the case of an E-field parallel to the long side. The position of the peaks and the FWHM can be tuned by changing the converging angle. Figure 2.4 shows that the location of the peak blue shifts nearly linearly as the converging angle decreases. Moreover, since the throat size varies as the converging angle changes, the magnitudes of the transmission peak and the FWHM increase as the angle increases. Interestingly, the change of magnitude with respect to the angle is nearly linear. For frequencies beyond the cut off frequency ω_c , the transmissions drop rapidly, indicating the potential application as band-pass filters.

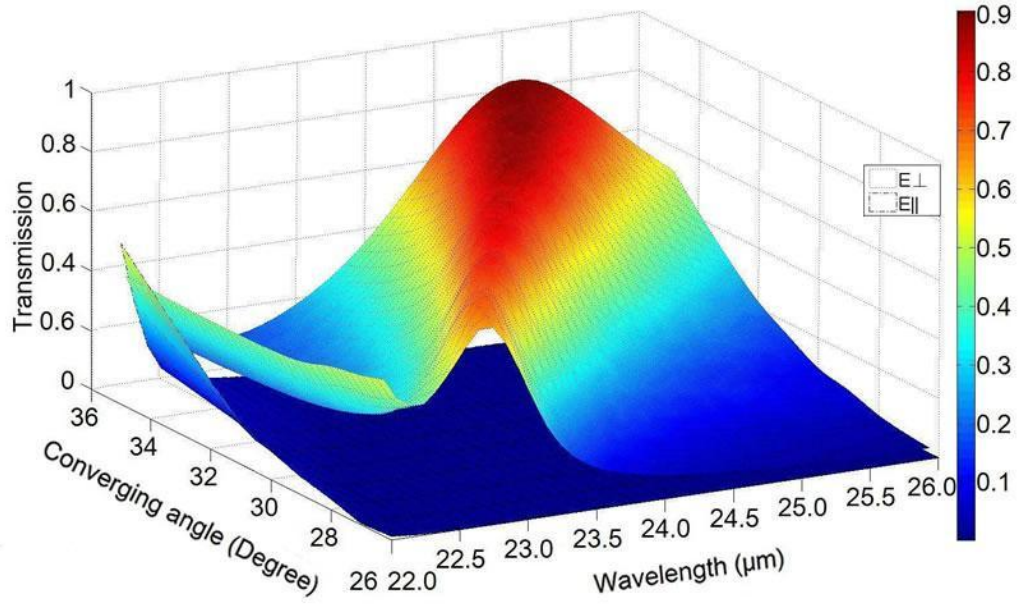


Figure 2.4: Transmissions for different converging angles. The hole area, film thickness and a/b ratio ($16\mu\text{m}/12\mu\text{m}$) remain the same in all cases.

2.3.3 Results for different metal film thickness

Figure 2.5 shows the transmission spectrum for Ag MHAs with different metal film thicknesses while keeping the same hole area, a/b ratio ($16\mu\text{m}/12\mu\text{m}$) and converging angle (30°). The solid and the dashed lines are for different polarizations. Similar to the results in sections 3.1 and 3.2, the transmissions are highly selective—there are strong transmission peaks only for the cases of E-field perpendicular to the long side. But the difference is that, since we extend our study to shorter wavelengths, there are two transmission peaks for some cases. As the thickness increases, one of the peaks stays almost at the same location ($\sim 21.8\mu\text{m}$), yet the location of the other peak blue shifts. The behavior of these two peaks may be due to the excitation of two types of electromagnetic modes as mentioned previously [24]: coupled SPPs and waveguide resonances. The

nearly fixed peaks are excited by coupled SPPs whose locations are not sensitive to the film thickness, whereas the other peaks are caused by the waveguide resonances.

From $t=2.0\mu\text{m}$ to $2.5\mu\text{m}$, the transmission peaks due to the waveguide resonances blue shift and both the magnitude and the FWHM of the peaks decrease resulting from the reduced throat area. However, the magnitudes of the peaks related to SPPs increase as the thickness increases. One possible reason is as the waveguide resonances peak blue shifts, the two peaks come closer and the interaction between them becomes stronger. When $t=2.5\mu\text{m}$, the interactions are so strong that the location of the SPPs peak red shifts a little. For the case of $t=3.0\mu\text{m}$, however, only the SPPs peak is left and it is relatively small (<0.5). This shows that without the contribution of the waveguide resonance, the magnitude of the SPPs peak will decrease with an increasing film thickness.

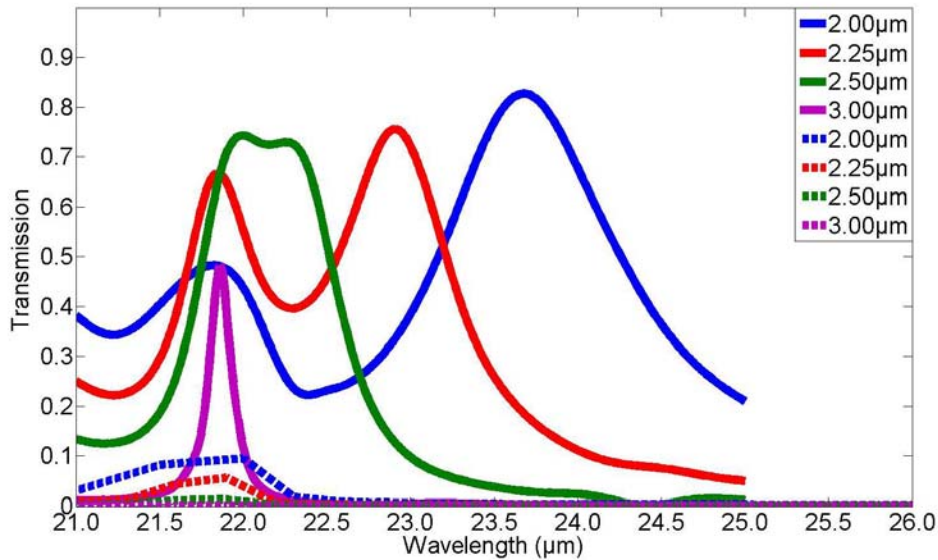


Figure 2.5: Transmissions for different metal film thickness. The hole area, converging angle (30°) and a/b ratio remain the same in all cases. The solid and dashed lines represent the transmissions for different polarizations.

2.4 CONCLUSION

The transmission spectrums of rectangular metallic hole arrays with different converging-diverging channels have been discussed in this paper. Since the structure is asymmetric along the x and y directions, it is highly selective for different polarizations, providing a potential application as a polarized optical filter. Meanwhile, by changing the a/b ratio, the converging angle and the metal film thickness, the transmission properties can be changed. As a result, this proposed RCDC shape in MHAs could lead to extraordinary transmission at different wavelengths and can be used to develop THz polarized filters. This could lead to a wide range of applications in tunable filters, photonic circuits, nanopatterning, and biosensors.

2.5 REFERENCES

1. T. W. Ebbesen, H. J. Lezec, H. F. Ghaemi, T. Thio, and P. A. Wolff, "Extraordinary optical transmission through sub-wavelength hole arrays," *Nature* 391, 667-669 (1998).
2. Q. Cao, and P. Lalanne, "Negative role of surface plasmons in the transmission of metallic gratings with very narrow slits," *Phys. Rev. Lett.* 88, 057403 (2002).
3. P. Lalanne, J. P. Hugonin, and J. C. Rodier, "Theory of surface plasmon generation at nanoslit apertures," *Phys. Rev. Lett.* 95, 263902 (2005).
4. H. J. Lezec, and T. Thio, "Diffracted evanescent wave model for enhanced and suppressed optical transmission through subwavelength hole arrays," *Opt. Express* 12, 3629-3651 (2004).
5. D. X. Qu, D. Grischkowsky, and W. L. Zhang, "Terahertz transmission properties of thin, subwavelength metallic hole arrays," *Opt. Lett.* 29, 896-898 (2004).
6. H. Cao, and A. Nahata, "Influence of aperture shape on the transmission properties of a periodic array of subwavelength apertures," *Opt. Express* 12, 3664-3672 (2004).
7. F. Miyamaru, and M. Hangyo, "Finite size effect of transmission property for metal hole arrays in subterahertz region," *Appl. Phys. Lett.* 84, 2742-2744 (2004).

8. J. F. O'Hara, R. D. Averitt, and A. J. Taylor, "Terahertz surface plasmon polariton coupling on metallic gratings," *Opt. Express* 12, 6397-6402 (2004).
9. A. K. Azad, Y. Zhao, and W. Zhang, "Transmission properties of terahertz pulses through an ultrathin subwavelength silicon hole array," *Appl. Phys. Lett.* 86 (2005).
10. J. G. Rivas, C. Schotsch, P. H. Bolivar, and H. Kurz, "Enhanced transmission of THz radiation through subwavelength holes," *Phys. Rev. B* 68 (2003).
11. C. Janke, J. G. Rivas, C. Schotsch, L. Beckmann, P. H. Bolivar, and H. Kurz, "Optimization of enhanced terahertz transmission through arrays of subwavelength apertures," *Phys. Rev. B* 69 (2004).
12. M. Tanaka, F. Miyamaru, M. Hangyo, T. Tanaka, M. Akazawa, and E. Sano, "Effect of a thin dielectric layer on terahertz transmission characteristics for metal hole arrays," *Opt. Lett.* 30, 1210-1212 (2005).
13. J. B. Pendry, L. Martin-Moreno, and F. J. Garcia-Vidal, "Mimicking surface plasmons with structured surfaces," *Science* 305, 847-848 (2004).
14. A. Degiron, H. J. Lezec, W. L. Barnes, and T. W. Ebbesen, "Effects of hole depth on enhanced light transmission through subwavelength hole arrays," *Appl. Phys. Lett.* 81, 4327-4329 (2002).
15. A. K. Azad, and W. L. Zhang, "Resonant terahertz transmission in subwavelength metallic hole arrays of sub-skin-depth thickness," *Opt. Lett.* 30, 2945-2947 (2005).
16. C. L. Pan, C. F. Hsieh, R. P. Pan, M. Tanaka, F. Miyamaru, M. Tani, and M. Hangyo, "Control of enhanced THz transmission through metallic hole arrays using nematic liquid crystal," *Opt. Express* 13, 3921-3930 (2005).
17. J. M. Steele, Z. W. Liu, Y. Wang, and X. Zhang, "Resonant and non-resonant generation and focusing of surface plasmons with circular gratings," *Opt. Express* 14, 5664-5670 (2006).
18. K. J. K. Koerkamp, S. Enoch, F. B. Segerink, N. F. van Hulst, and L. Kuipers, "Strong influence of hole shape on extraordinary transmission through periodic arrays of subwavelength holes," *Phys. Rev. Lett.* 92 (2004).
19. A. Battula, Y. L. Lu, R. J. Knize, K. Reinhardt, and S. C. Chen, "Tunable transmission at 100 THz through a metallic hole array with a varying hole channel shape," *Opt. Express* 15, 14629-14635 (2007).
20. E. D. Palik, *Handbook of Optical Constants of Solids* (Academic, 1985).

21. COMSOL 3.3 Reference Manual, version 3.3 ed. (Comsol AB, 2006).
22. A. Lavrinenko, P. I. Borel, L. H. Frandsen, M. Thorhauge, A. Harpoth, M. Kristensen, T. Niemi, and H. M. H. Chong, "Comprehensive FDTD modelling of photonic crystal waveguide components," *Opt. Express* 12, 234-248 (2004).
23. A. R. Zakharian, M. Mansuripur, and J. V. Moloney, "Transmission of light through small elliptical apertures," *Opt. Express* 12, 2631-2648 (2004).
24. J. A. Porto, F. J. Garcia-Vidal, and J. B. Pendry, "Transmission resonances on metallic gratings with very narrow slits," *Phys. Rev. Lett.* 83, 2845-2848 (1999).

Chapter 3: Conclusion and Future Directions

3.1 SUMMARY

Plasmonic properties of subwavelength structures and developing new design for plasmonic optical devices have been explored in this thesis. Tuning the polarization-selective extraordinary transmission in the terahertz range has been achieved by introducing the RCDC structure.

In the thesis it was shown that with metallic holes having rectangular converging-diverging channels (RCDC) the transmission peaks can be selected by varying the a/b ratios, the converging angles, and the film thickness. The transmission of light with different polarizations can be tuned by changing the a/b ratios as well.

The transmission spectrum changes as the a/b ratio increases, but the magnitude of the transmission peak remains the same. Decreasing the a/b ratio causes an increase in the FWHM of the transmission peaks accompanied by a red-shift. As the converging angle decreases, location of the peak blue shifts nearly linearly. Moreover, since the throat size varies as the converging angle changes, the magnitudes of the transmission peak and the FWHM increase as the angle increases. Interestingly, the change of magnitude with respect to the angle is nearly linear. In the study of different metal film thickness, since we extend our study to shorter wavelengths, there are two transmission peaks for some cases. As the thickness increases, one of the peaks stays almost at the same location, yet the location of the other peak blue shifts. The behavior of these two peaks may be due to the excitation of two types of electromagnetic modes: coupled SPPs and waveguide resonances. The nearly fixed peaks are excited by coupled SPPs whose locations are not sensitive to the film thickness, whereas the other peaks are caused by the waveguide resonances. The asymmetry from the rectangular shape gives this structure

high selectivity for light with different polarizations and this selectivity is tunable by varying the a/b ratio. Furthermore, the RCDC shape gives extra degrees of geometrical variables to 2D-MHA for tuning the location of the transmission peak and FWHM. The tunable transmission property of this structure shows promise for applications in tunable filters, photonic circuits, and biosensors.

3.2 FUTURE WORK

In the field of plasmonics there are still lots of research opportunities to explore and develop. By employing tunable materials –whose dielectric constant can be controlled by temperature or electric field, the new design proposed and analyzed in this thesis may open a chance to implement the SPs based circuits, where electronics could merge with photonics at the nanoscale [1] for developing ultra-low loss optically functional device and couple them into non-conventional plasmonic chips. Hence it would be of significant interest to fabricate these new plasmonic optical devices and conduct experiments to confirm the tunable optical filters with fine properties.

On the other hand, exploitation of surface plasmons to improve the performance of solar cells has been drawing a lot of attentions recently. There are two factors SPs can help to enhance the absorption in thin film solar cell. First, the scattering of light at the nanostructures will help increasing the light path in the absorbing film. Second, the extraordinary high local electromagnetic field caused by the SPs will result in significant enhancement of absorption. Metallic nanoparticles and grating structures were introduced to both crystalline and amorphous silicon solar cells, either on the top or back surface of the absorbing layer [2-6]. Since SPs only occur at certain wavelengths, the absorption enhancement can be only achieved around these wavelengths. For the other wavelengths however, the absorption will even be decreased induced by the reflection and absorption

by the metals. How to realize broadband enhancement in a visible wavelength range remains a great challenge.

3.3 REFERENCES

1. E. Ozbay, "Plasmonics: Merging photonics and electronics at nanoscale dimensions," *Science*, 311, 189-193 (2006).
2. S. Pillai, K. R. Catchpole, T. Trupke, and M. A. Green, "Surface plasmon enhanced silicon solar cells," *J. Appl. Phys.*, 101, 093105 (2007).
3. D. M. Schaadt, B. Feng, and E. T. Yu, "Enhanced semiconductor optical absorption via surface plasmon excitation in metal nanoparticles," *Appl. Phys. Lett.*, 86, 063106 (2005).
4. D. Derkacs, S. H. Lim, P. Matheu, W. Mar, and E. T. Yu, "Improved performance of amorphous silicon solar cells via scattering from surface plasmon polaritons in nearby metallic nanoparticles," *Appl. Phys. Lett.*, 89, 093103 (2006).
5. Vivian E. Ferry, Luke A. Sweatlock, Domenico Pacifici, and Harry A. Atwater, "Plasmonic Nanostructure Design for Efficient Light Coupling into Solar Cells," *Nano Lett.*, 2008, 8 (12).
6. Florian Hallermann, Carsten Rockstuhl, Stephan Fahr, Gerhard Seifert, Stefan Wackerow, Heinrich Graener, Gero v. Plessen, and Falk Lederer, "On the use of localized Plasmon polaritons in solar cells," *phys. stat. sol. (a)* 205, No. 12, 2844–2861 (2008).

Bibliography

- A. Battula, Y. L. Lu, R. J. Knize, K. Reinhardt, and S. C. Chen, "Tunable transmission at 100 THz through a metallic hole array with a varying hole channel shape," *Opt. Express* 15, 14629-14635 (2007).
- A. Degiron, H. J. Lezec, W. L. Barnes, and T. W. Ebbesen, "Effects of hole depth on enhanced light transmission through subwavelength hole arrays," *Appl. Phys. Lett.* 81, 4327-4329 (2002).
- A. K. Azad, and W. L. Zhang, "Resonant terahertz transmission in subwavelength metallic hole arrays of sub-skin-depth thickness," *Opt. Lett.* 30, 2945-2947 (2005).
- A. K. Azad, Y. Zhao, and W. Zhang, "Transmission properties of terahertz pulses through an ultrathin subwavelength silicon hole array," *Appl. Phys. Lett.* 86 (2005).
- A. Lavrinenko, P. I. Borel, L. H. Frandsen, M. Thorhauge, A. Harpoth, M. Kristensen, T. Niemi, and H. M. H. Chong, "Comprehensive FDTD modelling of photonic crystal waveguide components," *Opt. Express* 12, 234-248 (2004).
- A. R. Zakharian, M. Mansuripur, and J. V. Moloney, "Transmission of light through small elliptical apertures," *Opt. Express* 12, 2631-2648 (2004).
- Atwater, H.A., The promise of plasmonics. *Scientific American*, 2007. 296(4): p. 56-63.
- Banerjee, M., Datta, S. K., Saha, H., 2005, "Enhanced optical absorption in a thin silicon layer with nanovoids," *Nanotechnology*, 16(9), pp. 1542-1548.
- Brown, C.A., et al., Unusual Monolayer Behavior of a Geminally Disubstituted Fatty-Acid - Characterization Via Surface-Plasmons and X-Ray Photoelectron-Spectroscopy Study. *Journal of Physical Chemistry*, 1983. 87(19): p. 3616-3619.
- C. Janke, J. G. Rivas, C. Schotsch, L. Beckmann, P. H. Bolivar, and H. Kurz, "Optimization of enhanced terahertz transmission through arrays of subwavelength apertures," *Phys. Rev. B* 69 (2004).
- C. L. Pan, C. F. Hsieh, R. P. Pan, M. Tanaka, F. Miyamaru, M. Tani, and M. Hangyo, "Control of enhanced THz transmission through metallic hole arrays using nematic liquid crystal," *Opt. Express* 13, 3921-3930 (2005).

- Chern, R., Liu, X., and Chang, C. 2007" Particle plasmons of metal nanospheres: Application of multiple scattering approach," Phys. Review E 76, pp. 016609.
- COMSOL 3.3 Reference Manual, version 3.3 ed. (Comsol AB, 2006).
- Craig, F. B. and Donld, R. H., 1983 Absorption and Scattering of Light by Small Particles, John Wiley & Sons, Canada, pp. 83-129.
- D. X. Qu, D. Grischkowsky, and W. L. Zhang, "Terahertz transmission properties of thin, subwavelength metallic hole arrays," Opt. Lett. 29, 896-898 (2004).
- E. D. Palik, Handbook of Optical Constants of Solids (Academic, 1985).
- Ebbesen, T.W., et al., Extraordinary optical transmission through sub-wavelength hole arrays. Nature, 1998. 391(6668): p. 667-669.
- F. Miyamaru, and M. Hangyo, "Finite size effect of transmission property for metal hole arrays in subterahertz region," Appl. Phys. Lett. 84, 2742-2744 (2004).
- Feringa, B. L., 2001, Molecular Switches Weinheim: Wiley–VCH , pp. 399
- Genet, C. and T.W. Ebbesen, Light in tiny holes. Nature, 2007. 445(7123): p. 39-46.
- H. Cao, and A. Nahata, "Influence of aperture shape on the transmission properties of a periodic array of subwavelength apertures," Opt. Express 12, 3664-3672 (2004).
- H. J. Lezec, and T. Thio, "Diffracted evanescent wave model for enhanced and suppressed optical transmission through subwavelength hole arrays," Opt. Express 12, 3629-3651 (2004).
- Han, L., Tang, T. and Chen, S., 2006, "Tuning the absorptions of Au nanospheres on a microshell by photo-deformation," Nanotechnology, 17, pp. 4600-4605.
- Innes, R.A. and J.R. Sambles, Optical Non-Linearity in Liquid-Crystals Using Surface Plasmon-Polaritons. Journal of Physics-Condensed Matter, 1989. 1(35): p. 6231-6260.
- J. A. Porto, F. J. Garcia-Vidal, and J. B. Pendry, "Transmission resonances on metallic gratings with very narrow slits," Phys. Rev. Lett. 83, 2845-2848 (1999).
- J. B. Pendry, L. Martin-Moreno, and F. J. Garcia-Vidal, "Mimicking surface plasmons with structured surfaces," Science 305, 847-848 (2004).
- J. F. O'Hara, R. D. Averitt, and A. J. Taylor, "Terahertz surface plasmon polariton coupling on metallic gratings," Opt. Express 12, 6397-6402 (2004).

- J. G. Rivas, C. Schotsch, P. H. Bolivar, and H. Kurz, "Enhanced transmission of THz radiation through subwavelength holes," *Phys. Rev. B* 68 (2003).
- J. M. Steele, Z. W. Liu, Y. Wang, and X. Zhang, "Resonant and non-resonant generation and focusing of surface plasmons with circular gratings," *Opt. Express* 14, 5664-5670 (2006).
- Jackson, J. D. 1999, *Classical Electrodynamics* 3rd ed John Wiley & Sons, USA, pp. 352-56.
- Johnson, P. B. and Christy, R. W., 1972, "Optical Constants of the Noble Metals," *Phys. Rev. B*, 6, pp. 4370-79.
- Johnstone, W., et al., *Fibre-Optic Polarizers and Polarizing Couplers*. *Electronics Letters*, 1988. 24(14): p. 866-868.
- K. J. K. Koerkamp, S. Enoch, F. B. Segerink, N. F. van Hulst, and L. Kuipers, "Strong influence of hole shape on extraordinary transmission through periodic arrays of subwavelength holes," *Phys. Rev. Lett.* 92 (2004).
- Kawata, S., 2001, *Near-Field Optics and Surface Plasmon Polaritons*, Springer, New York.
- Kittel, C., 1971, *Introduction to Solid State Physics* 4th ed. Wiley Canada, pp. 248.
- Kovacs, G.J., Sulfide Formation on Evaporated Ag Films. *Surface Science*, 1978. 78(1): p. L245-L249.
- Kreibig, U. and Vollmer, M., 1995 *Optical Properties of Metal Clusters*, Springer, New York.
- M. Tanaka, F. Miyamaru, M. Hangyo, T. Tanaka, M. Akazawa, and E. Sano, "Effect of a thin dielectric layer on terahertz transmission characteristics for metal hole arrays," *Opt. Lett.* 30, 1210-1212 (2005).
- Mackowski, D. W. 1991 "Analysis of Radiative Scattering for Multiple Sphere Configurations," *Proceedings: Mathematical and Physical Sciences*, 433 (1889), pp. 599-614.
- Maier, S.A. and H.A. Atwater, *Plasmonics: Localization and guiding of electromagnetic energy in metal/dielectric structures*. *Journal of Applied Physics*, 2005. 98(1).
- Maier, S.A., *Plasmonics: Fundamentals and Applications*. 1 edition ed. 2007: Springer. 223.

- Martinot, P., S. Laval, and A. Koster, Optical Bistability from Surface-Plasmon Excitation through a Nonlinear Medium. *Journal De Physique*, 1984. 45(3): p. 597-600.
- Mie, G., 1908 "Beiträge zur Optik trüber Medien speziell kolloidaler Metallösungen," *Ann. Phys.* 25, pp. 376-445.
- Mie, G., Articles on the optical characteristics of turbid tubes, especially colloidal metal solutions. *Annalen Der Physik*, 1908(25).
- Mulvaney, P., Not all that's gold does glitter. *Mrs Bulletin*, 2001. 26(12): p. 1009-1014.
- Otto, A., Excitation of nonradiative surface plasma waves in silver by method of frustrated total reflection. *Zeitschrift Fur Physik*, 1968(216): p. 398.
- P. Lalanne, J. P. Hugonin, and J. C. Rodier, "Theory of surface plasmon generation at nanoslit apertures," *Phys. Rev. Lett.* 95, 263902 (2005).
- Palmer, K. F. and Williams, D., 1974, *J. Opt. Soc. Am.* 64, pp. 1107.
- Pockrand, I., Surface Plasma-Oscillations at Silver Surfaces with Thin Transparent and Absorbing Coatings. *Surface Science*, 1978. 72(3): p. 577-588.
- Q. Cao, and P. Lalanne, "Negative role of surface plasmons in the transmission of metallic gratings with very narrow slits," *Phys. Rev. Lett.* 88, 057403 (2002).
- Raether, H., *Surface Plasmons on Smooth and Rough Surfaces and on Gratings*. 1988: Springer-Verlag. 136 pages.
- Rechberger, W., Hohenau, A., Leitner, A., Krenn, J.R., Lamprecht, B., and Aussenegg, F.R., 2003, "Optical properties of two interacting gold nanoparticles," *Optics Communications* 220, pp. 137–141.
- Ritchie, R.H., Plasma losses by fast electrons in thin films. *PHYSICAL REVIEW* 1957(106).
- Sambles, J.R., G.W. Bradbery, and F.Z. Yang, Optical-Excitation of Surface-Plasmons - an Introduction. *Contemporary Physics*, 1991. 32(3): p. 173-183.
- Segelstein, D., 1981, "The Complex Refractive Index of Water," M.S. Thesis, University of Missouri, Kansas City, Missouri, USA.
- Shvalagin, V. V., Stroyuk, A. L., and Kuchmii, S. Y., 2007, "Photochemical synthesis of ZnO/Ag nanocomposites," *J. Nanoparticle Research*, 9(3), pp. 427-440.

- T. W. Ebbesen, H. J. Lezec, H. F. Ghaemi, T. Thio, and P. A. Wolff, "Extraordinary optical transmission through sub-wavelength hole arrays," *Nature* 391, 667-669 (1998).
- Vandenbem, C. and Vigneron, J. P., 2005, "Mie resonances of dielectric spheres in face-centered cubic photonic crystals," *J. Opt. Soc. Am. A*, 22 (6), pp. 1042-47.
- Weaver, J. H. and Frederikse, H. P. R. 2001, *Optical Properties of Selected Elements* (82 Ed), CRC Press, Boca Raton, FL, USA.
- Wikipedia. Finite element method. Available from: http://en.wikipedia.org/wiki/Finite_Element_Method.
- Wikipedia. Plasmon. Available from: <http://en.wikipedia.org/wiki/Plasmonics>.
- Yee, K.S., Numerical solution of initial boundary value problems involving Maxwell's equations in isotropic media. *IEEE Trans. Antennas Propag.*, 1966(14).
- Yee, S.S., J. Homola, and G. Gauglitz, Special issue: Surface plasmon resonance (SPR) optical sensors, current technology and applications - Preface. *Sensors and Actuators B-Chemical*, 1999. 54(1-2): p. 1-1.
- E. Ozbay, "Plasmonics: Merging photonics and electronics at nanoscale dimensions," *Science*, 311, 189-193 (2006).
- S. Pillai, K. R. Catchpole, T. Trupke, and M. A. Green, "Surface plasmon enhanced silicon solar cells," *J. Appl. Phys.*, 101, 093105 (2007).
- D. M. Schaadt, B. Feng, and E. T. Yu, "Enhanced semiconductor optical absorption via surface plasmon excitation in metal nanoparticles," *Appl. Phys. Lett.*, 86, 063106 (2005).
- D. Derkacs, S. H. Lim, P. Matheu, W. Mar, and E. T. Yu, "Improved performance of amorphous silicon solar cells via scattering from surface plasmon polaritons in nearby metallic nanoparticles," *Appl. Phys. Lett.*, 89, 093103 (2006).
- Vivian E. Ferry, Luke A. Sweatlock, Domenico Pacifici, and Harry A. Atwater, "Plasmonic Nanostructure Design for Efficient Light Coupling into Solar Cells," *Nano Lett.*, 2008, 8 (12).
- Florian Hallermann, Carsten Rockstuhl, Stephan Fahr, Gerhard Seifert, Stefan Wackerow, Heinrich Graener, Gero v. Plessen, and Falk Lederer, "On the use of localized Plasmon polaritons in solar cells," *phys. stat. sol. (a)* 205, No. 12, 2844–2861 (2008).

Vita

Wei Wang was born in Shijiazhuang, Hebei Province, China on July 24th 1983, son of Mr. Shulin Wang and Mrs. Yanmin Li. After finishing from Tsinghua High School, he attended Tsinghua University, China to pursue his Bachelors in Automation. After that he further wanted to do graduate study and got into the University of Texas at Austin. Where, he did his research work in the general area of nanoscience and nanotechnology but with special emphasis in nano-optics.

Permanent address: Fengtai, Beijing, China, 100073

This thesis was typed by the author.